Using neutron star observations to determine crust thicknesses, moments of inertia, and tidal deformabilities

A. W. Steiner, S. Gandolfi, F. J. Fattoyev, and W. G. Newton

Using Neutron Star Observations to Determine Crust Thicknesses, Moments of Inertia, and Tidal Deformabilities

A. W. Steiner,[1] S. Gandolfi,[2] F. J. Fattoyev,[3] and W. G. Newton[3]

[1]*Institute for Nuclear Theory, University of Washington, Seattle, WA 98195*
[2]*Theoretical Division, Los Alamos National Laboratory, Los Alamos, NM 87545*
[3]*Department of Physics and Astronomy, Texas A&M University-Commerce, Commerce, Texas 75429, USA*

We perform a systematic assessment of models for the equation of state (EOS) of dense matter in the context of recent neutron star mass and radius measurements to obtain a broad picture of the structure of neutron stars. We demonstrate that currently available neutron star mass and radius measurements provide strong constraints on moments of inertia, tidal deformabilities, and crust thicknesses. A measurement of the moment of inertia of PSR J0737-3039A with 10% error, without any other information from observations, will constrain the EOS over a range of densities to within 50-60%. We find tidal deformabilities between 0.6 and 6×10^{36} g cm^2 s^2 (to 95% confidence) for $M = 1.4 \mathrm{M}_\odot$, and any measurement which constrains this range will provide an important constraint on dense matter. The crustal fraction of the moment of inertia can be as large as 10% for $M = 1.4 \mathrm{M}_\odot$ permitting crusts to have a large enough moment of inertia reservoir to explain glitches in the Vela pulsar even with a large amount of superfluid entrainment. Finally, due to the uncertainty in the equation of state, there is at least a 40% variation in the thickness of the crust for a fixed mass and radius, implying that future simulations of the cooling of a neutron star crust which has been heated by accretion will need to take this variation into account.

I. INTRODUCTION

Recent neutron star (NS) mass and radius observations have provided new constraints on the neutron star mass-radius curve and on the equation of state (EOS) of dense matter [1]. The EOS, in turn, is a fundamental property of quantum chromodynamics (QCD), probing cold and dense matter which is otherwise difficult to access in experiment.

In the near future, mass and radius observations may be complemented by other constraints on NS structure. While thousands of pulsars have been observed, there is only one binary system where both NSs are radio-active pulsars, PSR J0737-3039. The ability to observe pulsations from both NSs and the extreme nature of the system [2, 3], enables a potential measurement of the moment of inertia, I, of one of the neutron stars [4]. Also, the Laser Interferometer Gravitational-Wave Observatory (LIGO) is expected to measure the gravitational wave signal from a NS merger within the near future [5], and a sufficiently large signal to noise observation will enable a measurement of the neutron star tidal deformability [6–11] (denoted by λ and sometimes also called "tidal polarizability"). It turns out these two types of new observations are intimately related: the moment of inertia of a NS is strongly correlated with its tidal deformability [12, 13].

NSs can accrete matter from main-sequence companions which results in the emission of X-rays and the heating of the NS crust. If the accretion stops (referred to as "quiescence" since the X-rays from accretion subside), then the cooling NS crust can be directly observed [14]. The timescale for this cooling is proportional to the square of the NS crust thickness [15], and thus the crust thickness is important for determining the properties of the crust from observations of crust cooling [16–19].

Another potential constraint of NS structure comes from pulsar glitches. Previous works [20–22] have shown that, if NS crusts are believed to be the location of the angular momentum reservoir which contributes to the glitch spin up, then a significant fraction of the NS's moment of inertia must lie in the superfluid component of the crust. Thus glitches are sensitive to the crustal fraction of the moment of inertia, denoted $\Delta I / I$.

Finally, many of these quantities are (at least weakly) correlated with the nuclear symmetry energy [23–25]. The nuclear symmetry energy is the difference between the energy per baryon of neutron matter and that of nuclear matter (we ignore quartic terms, see Ref. [26]). We denote the symmetry energy, $S(n_B)$, where n_B is the baryon number density, and $S \equiv S(n_0)$ where n_0 is the nuclear saturation density. The quantity $3n_0 S'(n_0)$ is denoted as L. The value of L determines the pressure of neutron-rich matter at the saturation density. The pressure of neutron-rich matter, in turn, is related to all of the above NS structure quantities given above.

For the first time, we use existing NS mass and radius observations to predict the expected ranges of NS properties such as moments of inertia, tidal polarizabilities and crustal thicknesses which are measurable by a diverse range of ongoing observational programs. We generate these expected ranges based on Monte Carlo simulations using parameterizations which explore the full variation which is possible given current uncertainties in the nature of dense matter. Our EOS models are based on recent progress in the microscopic calculation of neutron-rich matter near the nuclear saturation density. At high densities, we assume no additional correlation with mat-

ter at lower densities, and use models which allow for strong phase transitions. Our method is in contrast to several previous works which have computed theoretical predictions of moments of inertia, crust thicknesses, and tidal polarizabilities for smaller samples of representative EOSs [1, 23, 27–34]. Future observations will consitute direct tests of the theoretical framework we use and of the systematics of current mass-radius observations.

II.   METHOD

For the first observational data set, we use (i) the five mass and radius measurements from photospheric radius expansion bursts in Ref. [35–38] (assuming that the photosphere is extended at "touchdown" as justified in Ref. [36]) and (ii) the five radius measurements from quiescent low-mass X-ray binaries in Refs. [39, 40] taking the hydrogen column densities and distances from the Harris catalog [41] and allowing for either hydrogen or helium atmospheres (this is the choice from Ref. [40] with the largest value for the evidence integral). The second data set additionally assumes a hypothetical 10% measurement of $I = (70\pm7)$ M$_\odot$ km^2 for a 1.4 M$_\odot$ NS. The centroid of this value is near that predicted by the mass-radius data (to allow easier comparison). The third type of data set includes only the I measurement (either 70 ± 7, 80 ± 8, or 90 ± 9 M$_\odot$ km^2) and no constraint from other mass and radius observations. Larger values of I would be implied by the radius constraint from long PRE bursts as suggested in Ref. [42].

There is a one-to-one correspondence between the NS mass-radius curve and the pressure as a function of energy density, $P(\varepsilon)$. We ensure that all EOSs are causal ($dP/d\varepsilon < 1$), hydrodynamically stable $dP/d\varepsilon > 0$, and also that all mass-radius curves produce a 2 solar mass NS in line with the recent mass measurements in Refs. [43, 44]. Strange quark matter is assumed not to be absolutely stable, so we consider only hybrid NSs where deconfined quark matter is surrounded by a hadronic crust, and leave the consideration of strange quark stars to future work. Moments of inertia are computed using the slowly-rotating (Hartle-Thorne) approximation [45, 46] and we use the correlation in Ref. [12, 13] to compute the tidal deformabilities. We have independently checked this correlation based on the expressions in Refs. [7, 47], and find that the correlation generally holds to within about 1% (since we are ignoring strange quark stars), though slightly larger variations can be generated with strong phase transitions just above the nuclear saturation density. However, such configurations, while not ruled out by the observational data, are finely-tuned and relatively improbable, and thus the results from the correlation are sufficient for our purposes.

There has been significant recent progress [48–50] on computing the EOS of neutron rich matter from using realistic nuclear forces, both quantum Monte Carlo and using chiral effective theory interactions in many-body per-

turbation theory. We assume that the binding energy of nuclear matter is -16 MeV, the saturation density is 0.16 fm^{-3} (typical values from Ref. [51]), and we choose limits for the incompressibility of 220 MeV $< K <$ 260 MeV from Refs. [52, 53]. Two different EOSs are employed near the nuclear saturation density. The first is the quantum Monte Carlo model from Ref. [48], and we refer to this model as "GCR". The limits 12.5 MeV $< a <$ 13.5 MeV and $0.47 < \alpha < 0.53$ are increased slightly from Ref. [54] to ensure that we include all possible models from Ref. [48]. These two parameters principally parameterize the two-nucleon part of the interaction. Additionally, we reparametrize b and β, parameters which control the three-nucleon interaction, in terms S and L. We limit S to between 29.5 MeV and 36.1 MeV in order to be consistent with the second model described below. We limit L to be between 30 and 70 MeV which covers the range of L from Ref. [48, 55]. We note that the GCR model is essentially a sum of two polytropes, with coefficients and exponents that were constrained by experiment.

For the second model, we use the parameterization from Ref. [49] ("HLPS"), and the results on neutron matter from Ref. [56] from an interaction based on chiral effective theory. At each point, we fix α, γ, η, the three parameters which control nuclear saturation, to fix the saturation density, the binding energy, and the incompressbility. Note that this α is distinct from the parameter with the same name in the GCR model. The remaining two parameters α_L and η_L, which control the properties of neutron matter, are again reparameterized in terms of S and L. The range on S from Fig. 1 of Ref. [56] is between 29.5 and 36.1 MeV and the range of L is between 44. and 65.0 MeV.

Both nuclear masses and theoretical models imply a correlation between S and L, thus we additionally restrict parameters to lie between (9.17 $S - 266$ MeV) $< L < (14.3\ S - 379$ MeV) which encloses the constraints from nuclear masses [51], quantum Monte Carlo [48], chiral interactions [56], and isobaric analog states [57] as summarized in Ref. [38]. The GCR and HLPS models are used only up to the nuclear saturation density, as they may not be valid if a phase transition is present. Increasing the density up to which we use these models would improve our constraints on the EOS but does not change the qualitative results. It is particularly critical that we assume no correlation between the EOS near the saturation density and the EOS at higher densities, except for the constraint that $P(\varepsilon)$ is a continuous and monotonically increasing function.

For the NS crust, we use the tabulated crust EOSs based on the work in Ref. [58]. The advantage of this crust EOS, relative to the older work in Ref. [59], is that we can employ the same values of S and L which we use in EOS of neutron-rich matter at the saturation density. A two-dimensional grid of crust EOSs with varying values of the S and L were computed and this grid was interpolated to generate the crust for general values of S and L in our simulations. For the transition between

the crust and the core, we use the correlation between n_t and S and L,

$$n_t = S_{30} \left(0.1327 - 0.0898 L_{70} + 0.0228 L_{70}^2 \right) \ \mathrm{fm}^{-3} \quad (1)$$

where L_{70} is L in units of 70 MeV and S_{30} is S in units of 30 MeV. For our ranges of S and L, this correlation gives transition densities between $0.06 \, \mathrm{fm}^{-3}$ and $0.1 \, \mathrm{fm}^{-3}$, consistent with those obtained in Ref. [60]. We use this transition density from Eq. 1 to compute the transition pressure, and find values between 0.30 and 0.82 $\mathrm{MeV/fm}^3$, slightly larger than the range 0.25 to 0.65 $\mathrm{MeV/fm}^3$ found in Ref. [1].

For the EOS above the saturation density, we either use a set of three piecewise polytropes (only five parameters since the transition to the first polytrope is already fixed by the EOS at the saturation density) referred to as "Model A" in Ref. [37]. Alternatively, we use a set of four line segments in the (ε, P) plane, "Model C" [37]. This latter model is useful because it provides an alternative model which tends to favor stronger phase transitions in the core. We do not employ Model B or Model D from Ref. [37] because they do not typically provide significantly different results from Model A at the current level of accuracy. The choice of either GCR or HLPS near saturation density and either Model A or Model C at high densities gives a total of four EOS models to use with our three data sets.

For each of the above data sets and EOS models, we perform a Markov chain Monte Carlo simulation as first outlined in Ref. [36]. To obtain our final results for a fixed data set we choose the smallest range which encloses all of the EOS models, as done in Ref. [37]. This procedure is a relatively simple version of a fully hierarchical Bayesian analysis which is currently too computationally expensive.

III. RESULTS

Results using GCR for matter near saturation density, Model A for higher densities, and using the mass-radius data described above are summarized in the second and third columns of Table I. For this particular model and data set, the results on non-rotating stars are very similar to those obtained previously [37, 54]. The moment of inertia ranges between 60 and 130 $\mathrm{M}_\odot \, \mathrm{km}^2$, with even smaller values for lower mass neutron stars. The fraction of the moment of inertia which lies in the neutron star crust is small, between 2 and 6% for 1.4 $\mathrm{M}_\odot$ neutron stars. The tidal deformability ranges between 0.2 and 2.6×10^{36} g cm^2 s^2, depending on mass. The HLPS model gives very similar neutron star radii in comparison to GCR. The numbers in the table outline the limits of probability distributions taken from the Monte Carlo. No assumption is made about the shape of the probability distribution, and the distributions can be significantly non-Gaussian.

A probability distribution for all of the relevant quantities can be generated for any combination of EOS model and neutron star data set, and 16 combinations are explored in this work. The variations among models and data sets is summarized in Table II which gives in 95% confidence limits for the radius of a 1.4 $\mathrm{M}_\odot$ neutron star. Model C gives smaller NS radii than Model A, due to the possible presence of phase transitions. A measurement of $I = 70$ implies slightly larger radii than that implied by the mass and radius data, which is the result of the fact that the mass and radius data prefers slightly smaller moments of inertia (i.e. columns four and five in Table I). Larger I measurements imply larger radii, as large as 14.7 km in some cases. These large neutron star radii are due to EOSs in which the pressure becomes significantly larger above the saturation density, but these are only likely if there is some systematic uncertainty which invalidates the mass and radius observations which were described above.

In order to allow more complete comparison between Model A and Model C, Table I tabulates the results for Model C for the same EOS at lower densities (GCR) and the same data set. The strong phase transitions implied by Model C lead to smaller pressures at low energy densities and higher pressures at high energy densities. This result originates in the constraints from observations, (which require small radii from low-mass neutron stars), and the constraint of a 2 solar mass neutron star (which requires a higher pressure at higher densities). Generally, radii, moments of inertia, and tidal deformabilities are smaller. Values of L are a potentially a bit larger in Model C; strong phase transitions permit a higher pressure near the saturation density because they make up for them with a lower pressure at higher densities. Constraints on S are not reported, because neutron star observations do not currently constrain S. The interplay between density regimes is difficult to observe in other studies which presume some sort of correlation between the nature of matter at saturation density and at higher densities.

Mass and radius observations suggest probability distributions for the moment of inertia of a 1.4 solar mass neutron star as given in the upper left panel of Fig. 1. It is clear that Model C, which favors stronger phase transitions gives slightly smaller values for $I(M = 1.4 \, \mathrm{M}_\odot)$ as expected. Among the four models which are plotted, the smallest 68% lower limit is 61.4 $\mathrm{M}_\odot \, \mathrm{km}^2$ and the largest 68% lower limit is 72.7 $\mathrm{M}_\odot \, \mathrm{km}^2$, i.e. a variation of less than 20%. The corresponding range for the radius of a 1.4 $\mathrm{M}_\odot$ NS is 10.6 to 12.1 km, comparable to results obtained previously [36, 37, 40, 54]. The relative size of the constraint on the pressure at an energy density of 450 $\mathrm{MeV/fm}^3$ from the $M - R$ data is 53%. On the other hand, since the systematic uncertainties of currently available mass and radius observations may be larger than that from a future I measurement, it is worth noting that a 10% I measurement alone constrains the pressure to within 55% at that same energy density and

Quantity (unit)	GCR, Mod. A, M&R data		GCR, Mod C, M& R data		GCR, Mod. A, $I = 90$	
	95% lower	95% upper	95% lower	95% upper	95% lower	95% upper
$P(\varepsilon = 300)$ (MeV/fm^3)	9.318	22.86	2.253	15.83	20.39	65.70
$P(\varepsilon = 450)$ (MeV/fm^3)	33.31	71.02	25.88	68.09	60.53	132.1
$P(\varepsilon = 600)$ (MeV/fm^3)	90.98	160.8	76.56	216.3	104.6	220.3
$P(\varepsilon = 1000)$ (MeV/fm^3)	281.0	413.0	260.9	558.1	260.4	461.2
L (MeV)	30.53	65.79	30.53	68.41	35.64	69.66
n_t (fm^{-3})	0.07142	0.09903	0.07168	0.1021	0.07061	0.09766
P_t (MeV/fm^3)	0.3125	0.8163	0.3149	0.7968	0.3119	0.8006
$\Delta R(n_t = 0.06, M = 1.4)$	0.6904	1.037	0.5949	0.9282	0.9550	1.488
$\Delta R(n_t = 0.08, M = 1.4)$	0.7455	1.206	0.6483	1.088	1.038	1.729
$\Delta R(n_t = 0.10, M = 1.4)$	0.8025	1.256	0.7073	1.136	1.136	1.863
$\Delta R(n_t = 0.08, M = 1.0)$	1.164	1.881	0.9457	1.651	1.539	2.383
$\Delta R(n_t = 0.08, M = 2.0)$	0.3411	0.6475	0.3252	0.6401	0.5420	1.154
$R(M = 1.4)$ (km)	10.79	12.44	10.22	11.87	12.39	14.47
$R(M = 1.7)$ (km)	10.74	12.40	10.31	11.95	12.36	14.82
$R(M = 2.0)$ (km)	10.16	12.25	10.10	12.01	11.96	15.13
$R_{\max}$ (km)	9.812	11.57	9.792	11.81	11.15	14.49
$n_{B,\max}$ (fm^{-3})	0.8770	1.234	0.7642	1.235	0.6059	0.9794
$\varepsilon_{\max}$ (MeV/fm^3)	1055	1597	578.4	1612	624.7	1236
$I(M = 1.4)$ (M$_\odot$ km^2)	60.62	77.06	56.25	69.87	(fixed)	
$I(M = 1.7)$ (M$_\odot$ km^2)	80.11	101.5	77.02	95.49	99.06	141.5
$I(M = 2.0)$ (M$_\odot$ km^2)	94.49	126.7	97.59	125.0	119.3	184.4
$(\Delta I/I)(n_t = 0.08, M = 1.4)$	0.02045	0.06084	0.01555	0.04723	0.03895	0.1033
$(\Delta I/I)(n_t = 0.08, M = 1.7)$	0.01284	0.03703	0.01033	0.03211	0.02346	0.07233
$(\Delta I/I)(n_t = 0.08, M = 2.0)$	0.006949	0.02317	0.006129	0.02231	0.01377	0.05424
$\lambda(M = 1.4)$	1.000	2.606	0.7306	1.811	1.945	5.904
$\lambda(M = 1.7)$	0.6596	2.067	0.5258	1.527	1.716	7.505
$\lambda(M = 2.0)$	0.2039	1.276	0.2635	1.211	0.6898	6.865

TABLE I: Predictions for the 95% confidence limits. The second and third columns show results for GCR, Model A, and the mass and radius data set. Within this particular model, the EOS is constrained to within about a factor of 2, and neutron star radii are constrained to around 1.5 km. Results for the HLPS model are very similar. Crust thicknesses, ΔR, are given in km and tidal deformabilities, λ, are given in units of 10^{36} g cm^2 s^2. The fourth and fifth column show results for Model C instead of Model A. Finally, the sixth and seventh columns use only a measurement of $I = 90 \pm 9$ M$_\odot$ km^2 for a 1.4 M$_\odot$ neutron star as a data set. This table summarizes the results for 3 the 16 combinations of models and data sets used in this paper.

to within 59% at an energy density of 1000 MeV/fm^3.

Current mass and radius observations imply tidal deformabilities for a 1.4 M$_\odot$ NS between (1.09 and 2.12)$\times 10^{36}$ g cm^2 s^2 to 68% confidence over all four EOS models. These provide guidance on how sensitive GW observatories will likely need to be in order to detect the tidal deformation in a double neutron star merger [7, 11]. This result is a natural consequence of rather small neutron star radii implied by the qLMXBs [39, 40]. Over all four EOS models none of the 95% confidence limits goes higher than 2.6 $\times 10^{36}$ g cm^2 s^2.

On the other hand, if we assume that the systematic uncertainties spoil mass and radius observations, tidal deformabilities can be larger. The 95% confidence limits of various quantities assuming a measurement of $I = (90\pm 9)$ M$_\odot$ km^2 are summarized in the sixth and seventh columns of Table I. This case shows tidal deformabilities can easily be as large as 7-8 $\times 10^{36}$ g cm^2 s^2, depending on mass. The most extreme 95% limits for the tidal deformability over all 16 combinations of models and data are 0.64 and 6.1 $\times 10^{36}$ g cm^2 s^2.

As shown in Fig. 2, we find a strong correlation between the radius of a 1.4 M$_\odot$ neutron star and the pressure at $\varepsilon = 300$ MeV/fm^3) approximately twice the nuclear saturation density (lower-left panel). There is a slightly weaker, and more model-dependent, correlation between $\Delta I/I$ and the transition pressure (upper-left panel), and the correlation between $\Delta I/I$ and L is extremely weak (upper-right panel), as found in Ref. [32]. There is a significant range in crust thicknesses due to the EOS, even for a fixed mass and radius, as shown in the lower-right panel.

Model	Radius for $M = 1.4$ M$_\odot$ (km)	
	95% lower limit	95% upper limit
GCR, Mod. A, M&R	10.79	12.44
GCR, Mod. C, M&R	10.22	11.87
HLPS, Mod. A, M&R	10.82	12.42
HLPS, Mod. C, M&R	10.21	11.86
GCR, Mod. A, M&R+$I = 70$	11.12	12.57
GCR, Mod. C, M&R+$I = 70$	10.47	12.03
HLPS, Mod. A, M&R+$I = 70$	11.13	12.49
HLPS, Mod. C, M&R+$I = 70$	10.50	12.09
GCR, Mod. A, $I = 70$	11.66	13.67
GCR, Mod. C, $I = 70$	10.55	13.47
HLPS, Mod. A, $I = 70$	11.66	13.43
HLPS, Mod. C, $I = 70$	10.64	13.64
GCR, Mod. A, $I = 80$	12.04	14.14
GCR, Mod. C, $I = 80$	11.36	14.41
GCR, Mod. A, $I = 90$	12.39	14.47
GCR, Mod. C, $I = 90$	10.59	14.68

TABLE II: Limits for the radius of a 1.4 M$_\odot$ neutron star for various models and data sets.
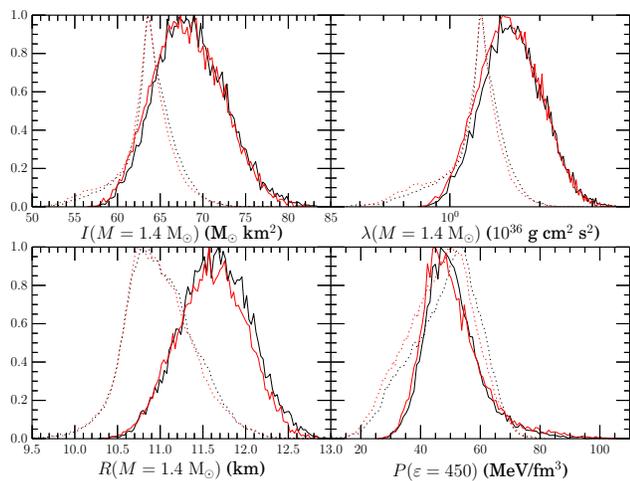
FIG. 1: Probability distributions for the moment of inertia of a 1.4 M$_\odot$ NS (upper left), tidal deformability of a 1.4 M$_\odot$ NS (upper right), radius of a 1.4 M$_\odot$ NS (lower left) and pressure at about three times the saturation density (lower right) given the set of mass and radius observations. Black lines are for GCR and red lines are for HLPS. Solid lines are for Model A and dotted lines are for Model C. Each of the distributions was separately normalized to have a maximum at 1.

IV. DISCUSSION

There is a quandary with pulsar glitches which originates in two results. The first is that some EOS models (like that of APR [61]) have small enough crusts that the fraction of the NS's moment of inertia contained in the crust is somewhat small ($\Delta I/I < 0.05$ for a 1.4 M$_\odot$ NS). The second is that there is a large amount of entrain-
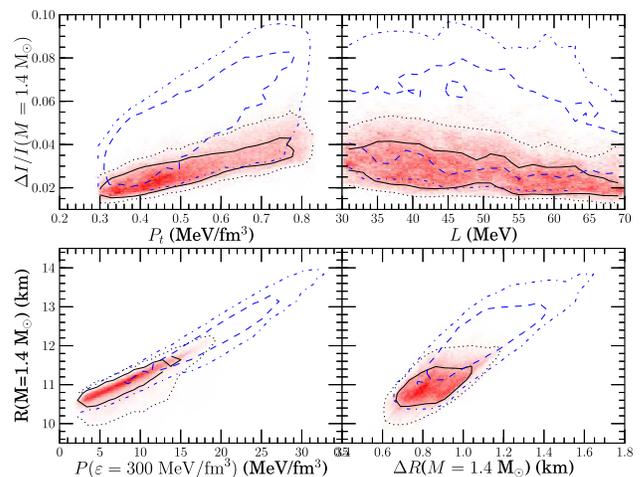
FIG. 2: Probability distributions for four pairs of quantities with EOS model GCR and Model C at high densities. In the upper-left panel, P_t is the pressure at the core-crust transition. All other quantities are defined in the text. The red density plot gives the probability distributions assuming the NS M and R data along with 68% contour lines (solid black) and 95% contour lines (dotted black). Also shown are the 68% (blue dashed) and 95% (blue dot-dashed) contour lines corresponding to the distribution given the third data set with only a measurement of $I = (70\pm7)$ M$_\odot$ km^2.

ment of superfluid neutrons by the lattice [62, 63], thus the amount of matter in the crust which is not strongly coupled to the lattice is only 15-25% of the total. Together, these limit the magnitude of pulsar glitches to be smaller than those already observed in the Vela pulsar which requires $\Delta I/I \geq 0.016$ [20–22, 64]. As can be seen in the upper-right of Fig. 2, NS mass and radius data predict a similar outcome, and the quandary stands. If we assume, however, that systematic uncertainties invalidate current mass and radius observations (as implied by Ref. [42]) and use our third data set which only contains a measurement of the moment of inertia of $I = (70\pm7)$ M$_\odot$ km^2, then we find many models with $\Delta I/I > 0.09$, as also shown in the upper-right panel. Smaller mass NSs give even larger values of $\Delta I/I$. As with the tidal deformabilities above, assuming a measurement of $I = (90\pm9)$ M$_\odot$ km^2 implies that $\Delta I/I$ could be larger than 0.10. Values as large as 0.11 can be obtained for lower mass neutron stars. These large values of $\Delta I/I$ can accommodate the observations of glitches in Vela even with the most extreme amounts of entrainment obtained in Ref. [62]. A similar conclusion has also been obtained independently in Ref. [65].

The thermal evolution of a NS crust as it cools depends on the hydrostatic structure of the crust (as well as on how photons and neutrons are transported). Frequently, crust cooling is studied using a small subset of the full variation possible for the hydrostatic structure [18, 19]. We find that, even for a fixed NS mass and radius, there is still considerable variation (due to the uncertainty in

the EOS of dense matter) in the thickness of the crust. This is shown in the lower right panel of Fig. 2, where the probability distribution of the radius of a 1.4 M$_\odot$ NS is plotted versus the crust thickness, ΔR. We find that, for a NS with an 11 km radius, the crust thickness varies by 42%. This means that a more complete variation of the parameter space may be required to determine the properties of the crust from crust cooling observations.

If a measurement of the moment of inertia of PSR J0737-3039A was far outside our predicted range, then that implies a conflict with the mass and radius observations. This conflict could be resolved with modification of strong-field GR. However, this modification may have to be finely tuned in order to modify the NS structure without spoiling the agreement with GR found in the observations of the post-Keplerian parameters in the PSR J0737-3039 system [66].

Current NS mass and radius observations are subject to several strong systematic uncertainties (as described in Refs. [36, 37, 40]) and a moment of inertia measurement outside our predicted range could shed light on these systematics. Our understanding of NS structure would be best served by several different kinds of observations with different systematic uncertainties so that no one effect could dominate the results. The same reasoning given above also holds true for measurements of tidal deformabilities, crust thicknesses, and crustal fractions of the moment of inertia. Also, there are other neutron star observations which we could have used, but these are unlikely to strongly modify our results. For example, there are constraints from pulse profile modeling on the neutron star PSR J0437-4715 [67], but these are more than likely consistent with our results so long as the mass of this particular star is near 1 M$_\odot$. In particular, the 68%

limit for the radius of a 1 M$_\odot$ from that measurement is 11.3 to 14 km, and this overlaps the ranges given for all of the models presented in Table I. The exception to this is if the systematic uncertainties in the qLMXB and PRE burst observations are so large that the associated constraints on mass and radius should be ignored *and* a moment of inertia measurement was made for a lower mass star which was relatively small (i.e. $I < 70$ M$_\odot$ km^2 for a 1.4 M$_\odot$ neutron star.

A large increase in the NS maximum mass, such as that implied by Refs. [68, 69], would significantly change these results. Larger maximum masses imply larger radii (larger pressure is needed at smaller densities in order to compete with gravity as the mass becomes larger), and thus larger moments of inertia and tidal deformabilities.

V. ACKNOWLEDGEMENTS

[1] J. M. Lattimer and M. Prakash, Astrophys. J. **550**, 426 (2001).
[2] M. Burgay, N. D'Amico, A. Possenti, R. N. Manchester, A. G. Lyne, B. C. Joshi, M. A. McLaughlin, M. Kramer, J. M. Sarkissian, F. Camilo, et al., Nature (London) **426**, 531 (2003).
[3] M. Kramer, I. H. Stairs, R. N. Manchester, M. A. McLaughlin, A. G. Lyne, R. D. Ferdman, M. Burgay, D. R. Lorimer, A. Possenti, N. D'Amico, et al., Science **314**, 97 (2006).
[4] T. Damour and G. Schäfer, Nuovo Cimento **101**, 127 (1988).
[5] J. Abadie and et al., Class. Quant. Grav. **27**, 173001 (2010).
[6] E. E. Flanagan and T. Hinderer, Phys. Rev. D **77**, 021502 (2008).
[7] T. Hinderer, B. D. Lackey, R. N. Lang, and J. S. Read, Phys. Rev. D **81**, 123016 (2010).
[8] T. Damour, A. Nagar, and L. Villain, Phys. Rev. D **85**, 123007 (2012).
[9] W. Del Pozzo, T. G. F. Li, M. Agathos, C. Van Den Broeck, and S. Vitale, Phys. Rev. Lett. **111**, 071101
(2013).
[10] J. S. Read, L. Baiotti, J. D. E. Creighton, J. L. Friedman, B. Giacomazzo, K. Kyutoku, C. Markakis, L. Rezzolla, M. Shibata, and K. Taniguchi, Phys. Rev. D **88**, 044042 (2013).
[11] B. D. Lackey, K. Kyutoku, M. Shibata, P. R. Brady, and J. L. Friedman, Phys. Rev. D **89**, 043009 (2014).
[12] K. Yagi and N. Yunes, Science **341**, 365 (2013).
[13] K. Yagi and N. Yunes, Phys. Rev. D **88**, 023009 (2013).
[14] R. E. Rutledge, L. Bildsten, E. F. Brown, G. G. Pavlov, V. E. Zavlin, and G. Ushomirsky, Astrophys. J. **580**, 413 (2002).
[15] J. M. Lattimer, K. A. van Riper, Madappa Prakash, and Manju Prakash, Astrophys. J. **425**, 802 (1994).
[16] W. H. G. Lewin and M. van der Klis, eds., *Compact Stellar X-Ray Sources* (Cambridge Univ. Press, Cambridge, England, 2006).
[17] P. S. Shternin, D. G. Yakolev, P. Haensel, and A. Y. Potekhin, Mon. Not. R. Astron. Soc. Lett. **382**, 43 (2007).
[18] E. F. Brown and A. Cumming, Astrophys. J. **698**, 1020 (2009).

[19] D. Page and S. Reddy, Phys. Rev. Lett. **111**, 241102 (2013).

[20] B. Link, R. I. Epstein, and J. M. Lattimer, Phys. Rev. Lett. **83**, 3362 (1999).

[21] N. Andersson, K. Glampedakis, W. C. G. Ho, and C. M. Espinoza, Phys. Rev. Lett. **109**, 241103 (2012).

[22] N. Chamel, Phys. Rev. Lett. **110**, 011101 (2013).

[23] A. W. Steiner, M. Prakash, J. M. Lattimer, and P. J. Ellis, Phys. Rep. **411**, 325 (2005).

[24] M. B. Tsang, J. R. Stone, F. Camera, P. Danielewicz, S. Gandolfi, K. Hebeler, C. J. Horowitz, J. Lee, W. G. Lynch, Z. Kohley, et al., Phys. Rev. C **86**, 015803 (2012), URL `http://link.aps.org/doi/10.1103/PhysRevC.86.015803`.

[25] B.-A. Li, A. Ramos, G. Verde, and I. Vidaña, Eur. Phys. J. A **50**, 1 (2014).

[26] A. W. Steiner, Phys. Rev. C **74**, 045808 (2006).

[27] V. Kalogera and D. Psaltis, Phys. Rev. D **61**, 024009 (1999).

[28] I. A. Morrison, T. W. Baumgarte, S. L. Shapiro, and V. R. Pandharipande, Astrophys. J. **617**, L135 (2004).

[29] M. Bejger, T. Bulik, and P. Haensel, Mon. Not. R. Astron. Soc. **364**, 635 (2005).

[30] J. M. Lattimer and B. F. Schutz, Astrophys. J. **629**, 979 (2005).

[31] J. M. Lattimer and M. Prakash, Phys. Rep. **442**, 109 (2007).

[32] F. J. Fattoyev and J. Piekarewicz, Phys. Rev. C **82**, 025810 (2010).

[33] F. J. Fattoyev, J. Carvajal, W. G. Newton, and B.-A. Li, Phys. Rev. C **87**, 015806 (2013).

[34] J. M. Lattimer and Y. Lim, Astrophys. J **771**, 51 (2013).

[35] F. Özel, G. Baym, and T. Güver, Phys. Rev. D **82**, 101301 (2010).

[36] A. W. Steiner, J. M. Lattimer, and E. F. Brown, Astrophys. J. **770**, 1 (2010).

[37] A. W. Steiner, J. M. Lattimer, and E. F. Brown, Astrophys. J. Lett. **765**, 5 (2013).

[38] J. M. Lattimer and A. W. Steiner, Eur. Phys. J. A **50**, 40 (2014).

[39] S. Guillot, M. Servillat, N. A. Webb, and R. E. Rutledge, Astrophys. J. **772**, 7 (2013).

[40] J. M. Lattimer and A. W. Steiner, Astrophys. J. **784**, 123 (2014).

[41] W. E. Harris, Astron. J. **112**, 1487 (1996).

[42] V. Suleimanov, J. Poutanen, M. Revnivtsev, and K. Werner, Astrophys. J **742**, 122 (2011).

[43] P. Demorest, T. Pennucci, S. Ransom, M. Roberts, and J. W. T. Hessels, Nature (London) **467**, 1081 (2010).

[44] J. Antoniadis et al., Science **340**, 448 (2013).

[45] J. B. Hartle, Astrophys. J. **150**, 1005 (1967).

[46] J. B. Hartle and K. S. Thorne, Astrophys. J. **153**, 807 (1968).

[47] S. Postnikov, M. Prakash, and J. M. Lattimer, Phys. Rev. D **82**, 024016 (2010).

[48] S. Gandolfi, J. Carlson, and S. Reddy, Phys. Rev. C **85**, 032801(R) (2012).

[49] K. Hebeler, J. M. Lattimer, C. J. Pethick, and A. Schwenk, Astrophys. J. **773**, 11 (2013).

[50] A. Gezerlis, I. Tews, E. Epelbaum, S. Gandolfi, K. Hebeler, et al., Phys.Rev.Lett. **111**, 032501 (2013), 1303.6243.

[51] M. Kortelainen, T. Lesinski, J. Moré, W. Nazarewicz, J. Sarich, N. Schunck, M. V. Stoitsov, and S. Wild, Phys. Rev. C **82**, 024313 (2010).

[52] S. Shlomo, V. Kolomietz, and G. Colò, Eur. Phys. J. A **30**, 23 (2006).

[53] J. Piekarewicz, J. Phys. G **37**, 064038 (2010).

[54] A. W. Steiner and S. Gandolfi, Phys. Rev. Lett. **108**, 081102 (2012).

[55] S. Gandolfi, J. Carlson, S. Reddy, A. W. Steiner, and R. B. Wiringa, Eur. Phys. J. A **50**, 1 (2014).

[56] I. Tews, T. Krüger, K. Hebeler, and A. Schwenk, Phys. Rev. Lett. **110**, 032504 (2013).

[57] P. Danielewicz and J. Lee, Nucl. Phys. A **922**, 1 (2014).

[58] W. G. Newton, M. Gearheart, and B.-A. Li, Astrophys. J. Suppl. **204**, 9 (2013).

[59] G. Baym, H. A. Bethe, and C. J. Pethick, Nucl. Phys. A **175**, 225 (1971).

[60] K. Oyamatsu and K. Iida, Phys. Rev. C **75**, 015801 (2007).

[61] A. Akmal, V. R. Pandharipande, and D. G. Ravenhall, Phys. Rev. C **58**, 1804 (1998).

[62] N. Chamel, Nucl. Phys. A **747**, 109 (2005).

[63] N. Chamel, Phys. Rev. C **85**, 035801 (2012).

[64] C. M. Espinoza, A. G. Lyne, B. W. Stappers, and M. Kramer, Mon. Not. R. Astron. Soc. **414**, 1679 (2011).

[65] J. Piekarewicz, F. Fattoyev, and C. Horowitz, Phys Rev. C. **90**, 015803 (2014).

[66] M. Kramer and N. Wex, Class. Quant. Grav. **26**, 073001 (2009).

[67] S. Bogdanov, Astrophys. J. **762**, 96 (2013).

[68] M. H. van Kerkwijk, R. P. Breton, and S. R. Kulkarni, Astrophys. J. **728**, 95 (2011).

[69] R. W. Romani, A. V. Filippenko, J. M. Silverman, S. B. Cenko, J. Greiner, A. Rau, J. Elliott, and H. J. Pletsch, Astrophys. J. Lett. **760**, L36 (2012).